

1
2
3
4
5
6
7
8
9
10
11
12
13
14
15
16
17
18
19
20
21
22

**A Statistically Optimal Analysis of Systematic Differences between Aeolus
HLOS Winds and NOAA’s Global Forecast System**

Hui Liu^{1,2}, Kevin Garrett¹, Kayo Ide³, Ross N. Hoffman^{1,2}, and Katherine E. Lukens^{1,2}

¹NOAA/NESDIS/Center for Satellite Applications and Research (STAR), College Park, MD
20740, USA

²Cooperative Institute for Satellite Earth System Studies (CISESS), University of Maryland,
College Park, MD 20740, USA

³University of Maryland, College Park, MD 20740, USA

Correspondence to: Kevin Garrett, NOAA/NESDIS/STAR, 5830 University Research Ct,
College Park, MD 20740, USA. Email: kevin.garrett@noaa.gov. Phone: (301) 683-3641.

Coauthor contact information:
Hui Liu: Hui.Liu@noaa.gov, ORCID 0000-0002-7959-0984.
Kevin Garrett: : kevin.garrett@noaa.gov, ORCID 0000-0002-7444-4363.
Kayo Ide: Kayo.Ide@noaa.gov, ORCID 0000-0001-5789-9326.
Ross N. Hoffman: Ross.N.Hoffman@noaa.gov, ORCID 0000-0002-4962-9438.
Katherine E. Lukens: Katherine.Lukens@noaa.gov.

23 **Key Points**

- 24
- 25
- 26
- 27
- 28
- 29
- 30
- There are speed-dependent systematic differences in the innovations of Aeolus Level-2B HLOS winds (B10) compared to short-term (6-h) FV3GFS forecasts.
 - The total least squares (TLS) regression provides a statistically optimal analysis of ~~the~~[these](#) differences.
 - A bias correction based on the TLS ~~bias~~-[analysis of these differences](#) proposed here is tested to optimize Aeolus wind assimilation and thus the impact of Aeolus winds on global forecasts.

31

32

33

34 **Abstract**

35 The European Space Agency Aeolus mission launched a first-of-its-kind spaceborne Doppler wind
36 lidar in August 2018. To optimize assimilation of the Aeolus Level-2B (B10) Horizontal Line-of-
37 Sight (HLOS) winds, significant systematic differences (~~hereafter biases~~) between the
38 observations and numerical weather prediction (NWP) background winds should be removed.
39 Total least squares (TLS) regression is used to estimate speed-dependent ~~biases~~systematic
40 differences between the Aeolus HLOS winds and the National Oceanic and Atmospheric
41 Administration (NOAA) Finite-Volume Cubed-Sphere Global Forecast System (FV3GFS) 6-h
42 forecast winds. Unlike ordinary least squares regression, TLS regression optimally accounts for
43 random errors in both predictors and predictands. Large well-defined, speed-dependent
44 ~~biases~~systematic differences are found in the lower stratosphere and troposphere in the tropics and
45 Southern Hemisphere. Correction of these ~~biases~~systematic differences improves the forecast
46 impact of Aeolus data assimilated into the NOAA global NWP system.

47

48 **Key words:** Aeolus winds, Doppler wind lidar, total least squares, bias correction

49

50 1 Introduction

51 The spaceborne Doppler wind lidar onboard the European Space Agency (ESA) Aeolus
52 mission measures both ~~Rayleigh (i.e., molecular) and Mie (i.e., clouds and aerosols)~~ and Rayleigh
53 (i.e., molecular) backscatter to derive wind profiles along the sensor's Horizontal Line of Sight
54 (HLOS) throughout the troposphere and lower stratosphere [Straume-Lindner, 2018; Straume et
55 al., 2020]. The Aeolus HLOS Level-2B (L2B) winds have demonstrated positive impacts on global
56 weather forecasts [Rennie et al., 2021; Cress, 2020; Garrett et al., 2020, ~~2021~~2022].

57 To optimize the positive impact of Aeolus HLOS winds on weather forecasts, large
58 systematic differences (~~hereafter biases~~) between Aeolus winds and numerical weather prediction
59 (NWP) model background winds should be corrected [Daley, 1991]. Therefore, it is important to
60 identify potential ~~biases~~systematic differences between Aeolus winds and their NWP model
61 background counterparts [Liu et al., 2020, 2021]. The ~~biases~~systematic differences may come from
62 both the NWP model background and the Aeolus winds. First, current operational global NWP
63 background winds still have larger errors or uncertainty in regions where conventional wind
64 observations are sparse or absent. For example, the 6-h forecast (~~background~~) zonal winds from
65 the ECMWF model (<https://www.ecmwf.int/en/forecasts>) and the NOAA Finite-Volume Cubed-
66 Sphere Global Forecast System (FV3GFS) model (<https://www.gfdl.noaa.gov/fv3/>) show large
67 systematic differences in the ~~zonal winds in the~~ upper troposphere and lower stratosphere of the
68 tropics, the Southern Hemisphere (SH), and ~~north~~poleward of 70° N, with maxima on the order of
69 2.0, -0.5, and 0.5 m/s, respectively (Fig. 1). ~~Differences in the use of satellite radiances at the NWP~~
70 ~~centers might contribute to the wind~~1). Such systematic differences in regions where conventional
71 data are sparse-

Commented [KL1]: Add a reference to the References section that includes this URL, and then cite that reference here.

Commented [RH2R1]: I think this is fine. It's not analogous to a document.

Commented [KL3]: See my previous comment

Commented [RH4R3]: Ditto.

72 may be due in part to differences in the assimilation of satellite radiances at the NWP
73 centers. Second, although corrections to several substantial bias-sources of systematic differences
74 in the Aeolus HLOS winds (baseline B10) have been implemented, including corrections to the
75 dark current signal anomalies of single pixels (so-called hot pixels) on the Accumulation-Charge-
76 Coupled Devices (ACCDs), to the linear drift in the illumination of the Mie and Rayleigh
77 spectrometers, and to the telescope M1 mirror temperature variations [Reitebuch et al., 2020;
78 Weiler et al., 2021], uncorrected biases systematic differences due to potential calibration issues
79 might remain in Aeolus HLOS winds and may contribute to potential biases systematic differences
80 between Aeolus and the NWP background HLOS winds. The residual biases systematic differences
81 may lead to sub-optimal assimilation of Aeolus HLOS winds in NWP systems.

82 NB: For clarity in the remainder of this article certain words and phrases are assigned
83 specific definitions. Thus, throughout this article, the phrase “Aeolus winds” specifically means
84 the observations of Aeolus Level-2B (B10) HLOS winds. Similarly, the phrase “FV3GFS winds”
85 specifically means the numerical weather prediction (NWP) background HLOS winds evaluated
86 from the FV3GFS 6-h forecasts at the observation location and time. (In discussions of winds that
87 are not HLOS winds, terms like u -wind, v -wind, or wind vector are used.) Further, the phrase “Mie
88 winds” specifically means Aeolus winds derived from Mie backscatter observations and the phrase
89 “Rayleigh winds” specifically means Aeolus winds derived from Rayleigh backscatter
90 observations. Also, throughout this article, the word “innovations” without further qualification
91 specifically refers to the differences between these Aeolus and FV3GFS winds, and the word
92 “bias” (as well as the phrases “Mie bias” and “Rayleigh bias”) without further qualification
93 specifically refers to the mean of these innovations, where the sample mean is over some specified
94 space-time volume for either the Mie or Rayleigh winds.

95 Speed-dependent biases ~~in Aeolus minus NWP background winds~~ identified and estimated
96 using ordinary least squares (OLS) ~~(i.e., in the innovations or O-B for the Aeolus wind~~
97 ~~observations)~~ are subject to contamination from random errors in Aeolus and/or ~~NWP~~
98 ~~background~~FV3GFS winds [Frost and Thompson, 2000], since OLS assumes no errors in the
99 predictor or independent variable, which in this case would be either the Aeolus ~~winds, the NWP~~
100 ~~background~~or FV3GFS winds, or a combination of the two. In contrast, total least squares (TLS)
101 regression accounts for errors in both dependent and independent variables and generates a
102 statistically optimal analysis of the biases [Deming, 1943; Ripley and Thompson, 1987;
103 Markovsky and Van Huffel, 2007]. For the case of Aeolus and ~~NWP background~~FV3GFS winds,
104 the use of linear TLS regression [Ripley and Thompson, 1987] finds a ~~best fit line that is~~ an optimal
105 estimate of the true (assumed linear) relationship between Aeolus and ~~NWP background~~FV3GFS
106 winds.

107 In this study, the TLS regression approach is used to estimate ~~potential linear speed-~~
108 ~~dependent~~ biases ~~between the Aeolus HLOS winds (B10) and the NOAA FV3GFS background~~
109 ~~winds that depend linearly on wind speed~~. The suboptimality of OLS bias estimates is demonstrated
110 by comparison to the TLS bias estimates, which are treated as “truth” in this study. A bias
111 correction based on the TLS bias analysis is proposed ~~for the mean differences of Aeolus minus~~
112 ~~FV3GFS winds in order~~ to optimize Aeolus wind assimilation ~~using~~by the FV3GFS model and
113 thus improve the impact of Aeolus winds on FV3GFS forecasts.

114 ~~Throughout this article, Aeolus and FV3GFS HLOS winds are referred to as Aeolus and~~
115 ~~FV3GFS winds, respectively. In discussions of winds that are not HLOS winds, terms like u wind,~~
116 ~~v wind, or wind vector are used.~~ Section 2 describes the Aeolus and FV3GFS ~~background~~ winds,

Commented [KL5]: Avoid “we” and its variations if at all possible

117 the TLS bias analysis method, and the estimation of the ratio of error variances of Aeolus ~~winds~~
118 to FV3GFS ~~background~~-winds, which ratio is used in the TLS regression. Section 3 describes the
119 variations of the TLS bias estimates with height, latitude, and wind speed. Section 4 demonstrates
120 the substantial differences between the TLS and OLS bias estimates. Section 5 proposes a TLS
121 bias correction for ~~O-B in~~ Aeolus data assimilation. The forecast impact of the TLS bias correction
122 is presented in Section 6. Section 7 presents a summary of findings and conclusions.

123 2 Data and Methodology

124 2.1 Aeolus L2B and FV3GFS background wind data

125 The Aeolus L2B cloudy-sky Mie winds and clear-sky Rayleigh ~~winds and cloudy sky Mie~~
126 winds are examined for the period 1-7 September 2019. This one-week period provides a sufficient
127 sample to estimate the biases. The Aeolus winds were obtained from the Aeolus dataset (baseline
128 B10) re-processed by ESA [Rennie et al., 2021, Weiler et al., 2021]. The reprocessing includes the
129 M1 bias correction, which removes most of the globally and vertically averaged biases of both
130 Mie and Rayleigh and Mie winds [Weiler et al., 2021]. The Aeolus winds are reported at a standard
131 set of vertical layers [de Kloe, 2019, 2020]. This study examines ~~Aeolus~~-Mie and Rayleigh winds
132 within height ranges of 0-22 km that include nearly all Aeolus ~~wind observations~~winds. The height
133 is defined relative to the EGM96 geoid for the L2B winds [Tan et al. 2008].

134 The Aeolus and FV3GFS winds are obtained from a data assimilation experiment
135 (hereafter the BASE experiment) where the Aeolus winds are monitored and the Aeolus wind
136 observation operator (H_i) is applied to the FV3GFS background (\mathbf{x}^b) to obtain the value of
137 FV3GFS wind ($y_i^b = H_i(\mathbf{x}^b)$) corresponding to each Aeolus wind (y_i^o). This experiment employs

138 the FV3GFS data assimilation system, called Global Statistical Interpolation [GSI, Kleist et al.
139 2009], configured for the 4DEnVar algorithm with 64 vertical levels, and horizontal resolutions of
140 C384 (~25 km) for the deterministic analysis and forecast and C192 (~50 km) for the 80 ensemble
141 members [Wang and Lei, 2014].

142 Similar Aeolus data quality control procedures as recommended by ESA and ECMWF
143 [Rennie et al., 2021] were implemented to reject the following observations: HLOS L2B
144 confidence flag “invalid”; Rayleigh winds at layers below 850 hPa, L2B uncertainties greater than
145 12 m/s, accumulation lengths less than 60 km, and atmospheric pressure within 20 hPa of
146 topographic surface pressure; Mie winds with L2B uncertainties greater than 5 m/s and
147 accumulation lengths less than 5 km. Further, a standard outlier check rejects any Aeolus wind for
148 which $|\Theta - B||y_i^o - y_i^b|$ is greater than 4 times the estimated errors for Aeolus winds prescribed by
149 the data assimilation system.

150 ~~The winds from Aeolus and collocated FV3GFS backgrounds are obtained from a data~~
151 ~~assimilation experiment (hereafter the BASE experiment) where the Aeolus winds are monitored~~
152 ~~and the Aeolus wind observation operator (H_*) is applied to the FV3GFS background (x^b) to~~
153 ~~obtain the value of FV3GFS background wind ($y_i^b = H_*(x^b)$) corresponding to each Aeolus~~
154 ~~observation (y_i^o). This experiment employs the FV3GFS data assimilation system, called Global~~
155 ~~Statistical Interpolation [GSI, Kleist et al. 2009], configured for the 4DEnVar algorithm with 64~~
156 ~~vertical levels, and horizontal resolutions of C384 (~25 km) for the deterministic analysis and~~
157 ~~forecast and C192 (~50 km) for the 80 ensemble members [Wang and Lei, 2014].~~

158 When examining Aeolus wind statistics, we stratify the Aeolus data by orbital phase, either
159 ascending when the spacecraft is moving northward or descending when the spacecraft is moving

160 southward. The vertical and daily variations of Mie and Rayleigh biases for global horizontal
161 means of Mie and Rayleigh winds minus FV3GFS background winds samples are consistent
162 throughout the period (Fig. 2). For the Mie winds at the ascending orbit orbits, the Mie biases are
163 positive above 6 km and negative below 6 km, and are as large as +1.8 m/s and -0.5 m/s,
164 respectively. The Mie biases are smaller and positive at most levels for the Mie winds in the
165 descending orbits. For Rayleigh winds In descending orbits, the Rayleigh biases are as positive as
166 +1.2 m/s above 10 km, and as negative as -1.2 m/s below 8 km. The positive biases in ascending
167 orbits are smaller. The results indicate that the biases vary substantially with height and orbit phase
168 for both Mie and Rayleigh winds. The mean differences of Mie and Rayleigh winds minus
169 FV3GFS winds biases also vary considerably with latitude (Fig. 3). Mie winds have biases are as
170 large positive as +1.5 m/s in the upper troposphere and Rayleigh winds have biases are as
171 large positive as +2.0 m/s in the tropical upper troposphere. Both Mie and Rayleigh winds show
172 biases are as negative biases as large as -1.0 m/s in the lowest layers.

173 The statistical relationship between Aeolus and FV3GFS winds is illustrated by the density
174 plots of collocated Aeolus and FV3GFS winds (in Fig. 4). There is a strong correlation of 0.93
175 between Mie and FV3GFS winds, and of 0.96 between Rayleigh and FV3GFS winds. The average
176 and OLS regression of the innovations (Aeolus versus FV3GFS winds) as a function of Aeolus
177 wind suggest considerable speed-dependent biases with both linear and non-linear components
178 (Fig. 5). In this study, we focus on the estimation and correction of the linear part of the biases
179 using the TLS linear regression.

180 2.2 TLS Linear Regression

181 In this section, we review the TLS linear regression method [Ripley and Thompson, 1987]
182 in the context of estimating potential speed-dependent biases ~~between Aeolus winds and FV3GFS~~
183 ~~background winds~~. The TLS estimate for each collocated pair of Aeolus and FV3GFS winds (y_i^o ,
184 y_i^b) is defined by

$$185 \quad y_i^o = \hat{y}_i^o + \varepsilon_i^o \quad \text{and} \quad y_i^b = \hat{y}_i^b + \varepsilon_i^b \quad (i=1, N) \quad (1)$$

186 where \hat{y}_i^o and \hat{y}_i^b are the TLS estimates of the true Aeolus and FV3GFS winds, ~~and~~ ε_i^o and ε_i^b are
187 random errors, and N is the number of Aeolus/FV3GFS wind collocations in the sample. The
188 sample might be defined by a vertical layer or a latitude band. In OLS regression, since it is
189 assumed that there are no errors in the predictor, the predictor can be used directly to estimate the
190 predictand. The situation is a little more complicated in TLS regression where $(\hat{y}_i^b, \hat{y}_i^o)$, the most
191 probable true state, is the point on the regression line that is closest in a statistical sense to the point
192 (y_i^b, y_i^o) .

193 Here it is assumed that ε_i^o and ε_i^b are independent and that the random error variance
194 ratio $\delta = (\sigma^o/\sigma^b)^2 = E[\varepsilon_i^o \varepsilon_i^o] / E[\varepsilon_i^b \varepsilon_i^b]$ is known. The error variance ratio δ is a crucial
195 parameter in determining the TLS bias analysis and is estimated as described in the next section.
196 Further, the true relationship between the Aeolus and FV3GFS winds is assumed to be described
197 by a linear function (as seen in Fig. 5):

$$198 \quad \hat{y}_i^o = c_0 + c_1 \hat{y}_i^b \quad (i=1, N) \quad (2)$$

199 where c_0 is an offset or constant bias coefficient and c_1 is a speed-dependent bias coefficient.

200 The TLS regression finds an optimal estimate of the \hat{y}_i^b , c_0 and c_1 by minimizing the cost
201 function J:

$$\begin{aligned} 202 \quad J &= \sum_{i=1}^N \left((\varepsilon_i^o / \sigma^o)^2 + (\varepsilon_i^b / \sigma^b)^2 \right) \\ 203 \quad &= \frac{1}{(\sigma^o)^2} \sum_{i=1}^N \left((y_i^o - c_0 - c_1 \hat{y}_i^b)^2 + \delta (y_i^b - \hat{y}_i^b)^2 \right) \end{aligned} \quad (3)$$

204 To determine the \hat{y}_i^b , the derivative of J with respect to \hat{y}_i^b is set to zero:

$$205 \quad \hat{y}_i^b = (c_1 (y_i^o - c_0) + \delta y_i^b) / (c_1^2 + \delta) \quad (i=1, N) \quad (4)$$

206 Eq. (4) thereby reduces the problem to a minimization in terms of c_0 and c_1 . A similar equation
207 holds even if the error variances vary with i , but then there is no closed form solution for c_0 and
208 c_1 , as there is in the current case, which is known as the Deming problem [Ripley and Thompson,
209 1987]. When the coefficients c_0 and c_1 are obtained, the TLS estimate for the new or within-sample
210 observation is given by Eq. (4). Finally, the estimate of the bias for the k th observation, either for
211 a new or within-sample observation, is given by

$$212 \quad \hat{d}_k = \hat{y}_k^o - \hat{y}_k^b = c_0 + (c_1 - 1) \hat{y}_k^b \quad (5)$$

213 Given the form of Eq. (5), we will refer to c_0 and $(c_1 - 1)$ as the ~~constant offset~~ and speed-
214 dependent bias coefficients, respectively, hereafter.

215 2.3 Estimation of the random error variance ratio

216 The random error variance ratio $\delta = (\sigma^o / \sigma^b)^2$ in the TLS bias analysis is estimated from
217 the innovations from the BASE experiment [for 1-7 September 2019](#) using the Hollingsworth-
218 Lonnberg (HL) method (Hollingsworth and Lonnberg, 1986; Garrett et al., [2021,2022](#)). It is

219 assumed that there are no correlations between the random errors of the Aeolus and FV3GFS
 220 winds, and no horizontal correlations between the random errors of Aeolus winds separated by
 221 more than 90 km. These assumptions are justified *a-posteriori* by the reasonable error estimate
 222 of FV3GFS background winds (Garrett et al., 2022).

223 ~~The~~ Global error estimates are calculated for all ~~Aeolus-Mie and Rayleigh~~ winds in each
 224 layer as follows. ~~The layers are defined by the global average heights of the Rayleigh and Mie~~
 225 ~~wind in each vertical range bin.~~ First, the spatial covariance of ~~Aeolus observation minus~~
 226 ~~background~~ the innovations is calculated. ~~Since these are innovations from the BASE experiment~~
 227 ~~where Aeolus data are not assimilated.~~ ~~Under the assumption,~~ it is reasonable to assume that the
 228 Aeolus and FV3GFS ~~background~~ wind errors are uncorrelated. ~~Then the spatial covariance of the~~
 229 ~~variance of Θ -Binnovations,~~ $(\sigma^{o-b})^2$, ~~at zero separation distance,~~ is equal to ~~the sum of the~~
 230 ~~variance of the random error of Aeolus winds and FV3GFS winds,~~

$$231 \quad (\sigma^{o-b})^2 = (\sigma^o)^2 + (\sigma^b)^2 \quad (6)$$

232 where σ^o and σ^b are the random error standard deviations of Aeolus ~~winds~~ and FV3GFS
 233 ~~background~~ winds, respectively.

234 By assumption, at separation distances greater than 90 km, the Θ -Binnovation covariances
 235 are estimates of the FV3GFS wind error covariance alone and can be extrapolated back to zero
 236 separation to get an estimate of the error variance of the FV3GFS winds, $(\sigma^b)^2$, and then, using
 237 Eq. (6), the error variance of the Aeolus winds, $(\sigma^o)^2$, may be determined. Note that this can only
 238 be done using Θ -Binnovation covariances at separation distances large enough to have negligible
 239 covariances between the Aeolus winds. Since the calculated Θ -Binnovation covariances are
 240 globally averaged over all ~~wind speeds~~ HLOS winds, it is not surprising that the

241 ~~remaining~~corresponding biases ~~for these~~ are small. The small residual biases in the innovations
242 may introduce small (< 0.1) spurious spatial ~~covariances or correlations~~ (< 0.09). ~~To reduce the~~
243 ~~impact of the biases, the~~ This spurious correlation, taken as the value calculated for the last bin
244 ~~(at the separation distance of 990 km is considered due to the biases and)~~ is removed from the
245 ~~correlations/covariances~~correlation curves at all separation distances. The estimated random error
246 variance ratio δ is ~~estimated at~~assigned to the middle layer center height of, defined as the global
247 average heights of the Mie and Rayleigh wind in each vertical range bin. ~~Fig. separately for Aeolus~~
248 Mie and Rayleigh samples for 1-7 September 2019. Figure 6 shows that the vertical profiles of the
249 square root of δ vary in the range of 1.2-1.6 ~~and 2-3~~ for Mie winds versus FV3GFS winds and and
250 2-3 for Rayleigh winds versus FV3GFS winds, respectively.

251 3 The TLS Bias Estimates

252 In this section, variations of the TLS bias estimates with orbital phase and height are
253 examined to ~~preface~~motivate the use of a TLS bias correction scheme proposed in Section 5.

254 3.1 Variation of TLS Bias Estimates with Height

255 The variation of the TLS solution with height and orbital phase is described here. The TLS
256 samples include winds at all latitudes in each layer. The vertical distribution of the TLS constant
257 and speed-dependent bias analysis coefficients in Eq. (5) is shown in ~~Figure~~Fig. 7. The speed-
258 dependent bias coefficient ($c_1 - 1$) varies substantially with height and orbital phase. For Mie
259 winds, ~~the~~this coefficient is quite large at most heights, ranging from 3% to 6%, with maxima at 3
260 km and 12-16 km. ~~The coefficient~~ For Rayleigh winds, this coefficient is smaller and ranges from

261 1% to 3% in ascending orbits and 1-5% in descending orbits, with maxima around the 3.5 km and
262 16 km.

263 The ~~constantoffset~~ bias coefficient c_0 for both Mie and Rayleigh winds also shows large
264 variations ~~on~~with height and orbit with its value as large as +/- 1.0 m/s. In general, the
265 ~~constantoffset~~ bias coefficient is positive in upper layers and negative in layers close to the Earth's
266 surface, consistent with the patterns seen in the global horizontal average of ~~the~~ innovations in
267 ~~FigureFig.~~ 2. The vertical distribution of the average TLS bias ~~estimatesestimate~~ as a function of
268 Aeolus wind is shown in ~~FigureFig.~~ 8. The biases vary substantially with height. Since the TLS
269 biases are in part dependent on speed, at most heights the biases increase substantially as the
270 magnitude of Aeolus wind speed increases. The biases at ~~highthe extreme~~ Aeolus wind speeds are
271 as large as +2.5 m/s and -1.0 m/s for Mie winds, and +1.5 m/s and -1.0 m/s for Rayleigh winds.
272 There are clear speed-dependent biases in the vertical average of these biases as well (Fig. 9). The
273 results suggest that the innovations have both vertically varying and vertically averaged speed-
274 dependent biases.

275 3.2 Variation of Biases with Latitude

276 The variation of the TLS solution with latitude and orbital phase is described here. ~~The~~
277 ~~TLS~~For this purpose, the samples ~~are separated by~~include all heights in each 10-degree latitude
278 ~~bands for all heights. band and~~ the vertical average of the error ratio δ is used ~~in the TLS bias~~
279 ~~estimates.~~ In general, the ~~bias~~ coefficients obtained are large and vary considerably with latitude
280 and orbital phase, with maxima found in the tropics (Fig. 10). For example, the speed-dependent
281 bias coefficient ($c_1 - 1$) for Mie winds in the tropics can be quite large, ranging ~~from 0% up~~ to a
282 maximum of 11%. ~~TheThis~~ coefficient (~~$c_1 - 1$~~) is smaller for Rayleigh winds, ranging from -1%

Commented [KL6]: Word choice

283 to 5%, with maxima found in the tropics. The offset bias coefficient c_0 for Mie winds also varies
284 considerably with latitude and orbit, ranging from -1.0 m/s to +1.6 m/s. The offset bias
285 coefficient c_0 is smaller for Rayleigh winds.

286 The latitudinal distribution of the average TLS bias as a function of Aeolus wind speed is
287 shown in FigureFig. 11. For both Mie and Rayleigh winds, the average TLS biases increase
288 considerably at most latitudes as the magnitude of Aeolus wind speed increases, particularly in the
289 tropics and SH, with maximaextreme values of about +/-1.5 m/s.

290 3.3 Discussion

291 The results indicate that the speed-dependent bias coefficient $(c_1 - 1)$ is quite large, with
292 $(c_1 - 1)$ reaching up to ~10% and 5% for Mie and Rayleigh winds, respectively, particularly in
293 the lower stratosphere and lower troposphere of the tropics. This suggests that there exist large
294 speed-dependent biases in the FV3GFS background winds and/or in the Aeolus winds. Given that
295 there exist large uncertainties in the FV3GFS (and ECMWF) background winds in the tropics (see
296 Fig. 1), it is likely that the FV3GFS background may be a significant source of the large biases,
297 and this will require further investigation. In any case, these large speed-dependent biases should
298 be corrected to optimize Aeolus wind assimilation and the impact of Aeolus winds on NWP
299 forecasts. The large variations of the TLS bias estimates onwith latitude and height provide a
300 guidance for guide the design of the proposed TLS bias correction in Section 5.

301 **4 Comparison to OLS Regressions**

302 Parallel OLS regressions using three different predictors of the biases ~~in O-B~~ are ~~conducted~~
303 ~~to compare~~ compared with the TLS bias estimate results presented in Section 3. The OLS predictors
304 are the FV3GFS winds, the Aeolus winds, and their average. The first two of these OLS regressions
305 are equivalent to OLS regressing Aeolus winds on FV3GFS winds and OLS regressing FV3GFS
306 winds on Aeolus winds.

307 ~~Note that when the error ratio $\delta \ll 1$ or $\gg 1$, the TLS solution becomes close to the OLS~~
308 ~~regression of the O-B on the Aeolus winds or on the FV3GFS winds, respectively. When ratio δ~~
309 ~~$= 1$, the TLS solution becomes equivalent to the OLS regression of the O-B on the average of~~
310 ~~Aeolus winds and FV3GFS winds. For example,~~ The regression lines of these two cases are added
311 to ~~Figure~~Fig. 4. The TLS speed-dependent coefficient ($c_1 - 1$) (in Eq. 5) is 6% and 4% for Mie
312 and Rayleigh winds, respectively. However, the OLS regression of Aeolus winds on FV3GFS
313 winds produces considerably smaller bias estimates, with ($c_1 - 1$) estimated as 1% and 2% for
314 Mie and Rayleigh winds, respectively. On the other hand, the OLS regression of the FV3GFS
315 winds on Aeolus winds exhibits much larger bias estimates relative to the TLS bias analysis, with
316 ($c_1 - 1$) estimated as 18% and 15% for Mie and Rayleigh winds, respectively.

317 The vertical distributions of the average biases as a function of Aeolus winds are shown in
318 ~~Figure~~Fig. 12 for the descending orbits for three methods: (1) OLS regression using FV3GFS
319 winds as a predictor (top row), (2) TLS regression (middle row, which repeats the bottom two
320 panels of Fig. 8), and (3) OLS regression using the average of FV3GFS and Aeolus as a predictor
321 (bottom row). The average bias estimates in the top panels are about 0.5 m/s smaller in magnitude
322 in most layers compared to the middle panels. The average biases in the bottom panels are about

323 0.5-1.0 m/s in magnitude larger than the middle panels in most layers, particularly for Rayleigh
324 winds. The bias estimates of OLS regression using Aeolus winds only as a predictor (not shown)
325 are even larger (than what is shown in the bottom panels). The large differences in the bias
326 estimates using the TLS and OLS regression are due to the fact that both Aeolus and FV3GFS
327 winds have large errors, and the fact that the errors of Aeolus winds are larger than FV3GFS
328 background winds. This leads to the different weightings of Aeolus winds and FV3GFS winds in
329 the TLS analysis (Eq. 3).

330 5 A TLS Bias Correction

331 In this section, a TLS bias correction for $\Theta-B$ is proposed to optimize Aeolus wind data
332 assimilation. Because the findings in Section 3 show substantial variation of the bias coefficients
333 with latitude, vertical layer, and orbital phase, the TLS bias coefficients are calculated from the
334 winds in 19 discrete bins of latitude (centered every 10° between 90° S to 90° N) for each vertical
335 range/layer and for ascending and descending orbits separately. The error ratio δ shown in Fig. 6
336 is used in all latitude bands for each layer.

337 ~~The corresponding TLS bias estimates show considerable speed dependent biases as well.~~
338 ~~For example, in the bins centered at the Equator and 80° S, where the speed dependent biases are~~
339 ~~the largest (see Fig. 9), the TLS bias estimates vary considerably with speed and in some cases are~~
340 ~~larger than ± 1.5 m/s at higher Aeolus speeds (Fig. 13).~~ For each assimilation cycle, the bias
341 coefficients are computed by TLS regression for the $\Theta-B$ innovations in the week before the cycle
342 (i.e., for the previous 28 cycles). One week provides a large enough sample for the regression. As
343 shown by Ripley and Thompson [1987], the TLS solution only involves solving a quadratic

344 equation with coefficients given by sample sums. Therefore, an efficient approach is to calculate
345 and save these sums for every cycle and accumulate them over the 28 cycles. For each of the
346 innovations in the assimilation cycle, values of the TLS regression coefficients c_0 and c_1 are
347 linearly interpolated to the latitude of the Aeolus observation. Subsequently, the TLS estimated
348 bias, calculated using Eq. (5), is subtracted from the innovation. Note that the bias correction is
349 determined by the TLS analysis solution for \hat{y}_k^b that in turn is determined from the observation and
350 background wind, y_k^o and y_k^b , following Eq. (4).

351 The proposed scheme is applied to the ~~innovations~~Aeolus and FV3GFS winds of the
352 BASE experiment. As expected, the corresponding TLS bias estimates show considerable speed-
353 dependent biases. For example, in the bins centered at the Equator and 80°S, where the speed-
354 dependent biases are expected to be largest based on Fig. 9, the TLS bias estimates vary
355 considerably with speed and in some cases are larger in magnitude than 1.5 m/s at higher Aeolus
356 wind magnitudes (Fig. 13). The vertical distribution of the average of the remaining biases (i.e.,
357 after TLS bias correction) as a function of Aeolus wind is shown in ~~Figure~~Fig. 14, which is in the
358 same format and for the same sample of observations as ~~Figure~~Fig. 8. A comparison of these two
359 figures reveals that most of the biases are removed by the proposed TLS bias correction. The
360 latitudinal variations of the biases are also corrected (Fig. 15). In addition, the biases in the
361 vertical average are also mostly removed, as shown in ~~Figure~~Fig. 9.

362 **6 Impact of the TLS bias correction on forecast skill**

363 Several Observing System Experiments (OSEs) using the NOAA global data
364 assimilation system are performed using the Aeolus winds with and without the TLS bias

365 correction. For the period of 2 August – 16 September 2019, Garrett et al., (2022) demonstrate
366 positive impact of Aeolus winds on NOAA global forecast. The largest impact is seen in the
367 tropical upper troposphere and lower stratosphere where the Day 1-3 wind vector forecast RMSE
368 is reduced by up to 4%. Additionally, the assimilation of Aeolus impacts the steering currents
369 ambient to tropical cyclones, resulting in up to a 20% reduction in track forecast error in the
370 Eastern Pacific and Atlantic basins. The application of TLS bias correction increases the positive
371 impact of Aeolus data assimilation on the forecasts.

372 OSE results for a 2019 record-breaking winter storm case over the US are reported here.
373 On 26 November 2019, one major storm approached the West Coast of the US from the Eastern
374 Pacific and produced a record-breaking low pressure of 973 hPa and wind gust of 171 km/h near
375 the Oregon/California border. Over the next few days, the low merged with the subtropical jet as
376 it tracked eastward across the US. The combination of cold air, moisture and high winds
377 produced snow blizzard conditions and hampered travel for millions across the US.

378 [As in Garrett et al., \(2022\)](#), the OSEs include the baseline experiment (BASE) without
379 the assimilation of Aeolus winds, the experiment AEOM that is identical to BASE except that
380 Aeolus winds are assimilated, and the experiment AEOT that is identical to AEOM ~~and except~~
381 ~~that it~~ also includes the ~~additional~~ TLS bias correction. ~~The setups of the OSEs are identical to~~
382 ~~those presented in Garrett et al. (2022)~~. A difference Summary Assessment Metric (SAM,
383 Hoffman et al., 2018) is computed for Day 1-7 forecasts of the experiments validated at 0000
384 UTC 22-28 November 2019. The SAM illustrates the overall forecast skill by normalizing the
385 AC and RMSE values for each parameter (temperature, geopotential height, wind, and relative
386 humidity) and each lead time. ~~In addition, the overall skills for AEOM and AEOT are compared~~

387 with respect to BASE in the North America (NA) region. ~~Figure~~Fig. 16 shows that the TLS bias
388 correction improves the impact of Aeolus winds on the forecasts of wind, temperature, and
389 geopotential height for Day 3-7 and especially for Day 5-7 lead times. The overall improvement
390 of Aeolus winds for AEOM and AEOT is about 4% and 10%, respectively (above the 95%
391 significance level, Fig. 16c), illustrating the usefulness of the TLS bias correction.

Commented [RH7]: Don't understand reference to NA region.

392 The vertically integrated water vapor transport (IVT) is a useful metric in forecasting
393 precipitation associated with winter storms (e.g., Lavers et al. 2017). The IVTs of the Day 7
394 forecast for the experiments validated and averaged for 0000 UTC November 26-28 are shown in
395 ~~Figure~~Fig. 17. Aeolus winds have a strong impact on the locations and intensities of the IVT
396 maxima near the US West Coast and in the Midwest. As a result, Aeolus winds show strong
397 impact on the locations and corresponding amounts of precipitation (~~Figure~~as seen in (Fig. 18),
398 ~~which correspond to~~and quantified by the Equitable Threat and BIAS skill scores, ~~respectively~~
399 (Fig. 19). Specifically, the precipitation amounts near the West Coast and the Midwest are much
400 less in AEOT than in BASE and AEOM. The precipitation in the Midwest also shifts eastward in
401 AEOT, compared to BASE and AEOM. The precipitation forecast skills (verified against
402 precipitation ~~analysis~~analyses) over the contiguous United States (CONUS) region, that is, the
403 Equitable Threat (location) and BIAS (amount) score, are shown in ~~Figure~~Fig. 19. The
404 precipitation amount is over-predicted (BIAS score > 1.0) in both BASE and AEOM, but is ~~more~~
405 ~~else~~closer to the analysis (BIAS score closer to 1.0) in AEOT. The Equitable Threat is larger
406 (with marginal significance level) in AEOT than in BASE and AEOM, indicating the location of
407 precipitation in the forecast is improved in AEOT. These results suggest potential benefit of the
408 TLS bias correction to ~~forecast of the~~precipitation forecasts.

Commented [KL8]: I would add something like this here, to really drive home why the location and amount are important. Also, are these scores widely known? Are they defined somewhere? Could you reference, and/or explain briefly how they're computed?

Commented [RH9R8]: Maybe <https://doi.org/10.1175/WAF-D-13-00087.1>

Commented [KL10]: Which analysis? Self or ECMWF?

409 7. Summary and Conclusions

410 In this study a TLS linear regression is used to optimally estimate speed-dependent linear
411 ~~biases between Aeolus L2B Horizontal Line of Sight winds and short term (6 h) forecasts of~~
412 ~~NOAA's FV3GFS. The~~ The Aeolus and FT3GFS winds for 1-7 September 2019 are analyzed.
413 Clear speed-dependent linear biases for both Mie and Rayleigh winds are found, particularly in the
414 lower troposphere and stratosphere of the tropics and Southern Hemisphere. The largest biases are
415 about 10% and 5% of FV3GFS wind speed and are as large as +/- 2.5 m/s and +/- 1.5 m/s at high
416 Aeolus wind ~~speed~~ magnitudes for Mie and Rayleigh winds, respectively.

417 It is found that the TLS linear bias estimates are considerably larger than the OLS
418 regression of Aeolus winds minus FV3GFS background winds on FV3GFS winds. However, they
419 are much smaller than the OLS regression both on Aeolus winds only and on the average of Aeolus
420 and FV3GFS winds. This is more evident for the Rayleigh winds.

421 The proposed TLS bias correction can remove much of the bias in the innovations before
422 Aeolus wind assimilation. In a companion paper, Garrett et al. [2022] demonstrate that the
423 application of this TLS bias correction considerably enhances the positive impact of Aeolus winds
424 on NOAA FV3GFS global and tropical cyclone forecasts for the period of 2 August to 15
425 September, 2019. In this study, it is also demonstrated that the application of the TLS bias
426 correction improves the impact of Aeolus winds on the forecast of a record-breaking 2019 winter
427 storm including the associated precipitation over the US. It is expected that the application of ~~this~~
428 ~~additional-the~~ TLS bias correction ~~to the innovations of Aeolus winds~~ can improve and enhance
429 Aeolus data impacts on the analysis and forecast skill of other NWP systems. It should be noted
430 that the proposed TLS approach presented here might be applied to other types of observations

431 that have errors typically characterized as a percentage of the observed value, including quantities
432 related to the concentrations or mass fractions of chemical species or hydrometeors, or quantities
433 like radio occultation refractivity and bending angle.

434 **Acknowledgments**

435 [The authors thank the two anonymous reviewers for their careful and helpful reviews.](#) This
436 work was supported by the NOAA/NESDIS Office of Projects, Planning, and Acquisition (OPPA)
437 Technology Maturation Program (TMP), managed by Patricia Weir and Dr. Nai-Yu Wang,
438 through the Cooperative Institute for Satellites and Earth System Studies (CISESS) at the
439 University of Maryland (Grant NA14NES4320003 and NA19NES4320002). The authors would
440 like to acknowledge Dr. Michael Rennie (ECMWF) and Dr. Lars Isaksen (KNMI) for their
441 comments and suggestions on the assimilation of Aeolus observations, and Dr. William McCarty
442 with NASA/GMAO for providing earlier versions of the GSI with Aeolus ingest and observation
443 operator capability. The Aeolus L2B BUFR data were provided by ECMWF. The scientific results
444 and conclusions, as well as any views or opinions expressed herein, are those of the author(s) and
445 do not necessarily reflect those of NOAA or the U.S. Department of Commerce.

446 **7 References**

447 Cress, A.: Validation and impact assessment of Aeolus observations in the DWD modeling
448 system. Status report'. *Aeolus NWP Impacts Working Meeting*, Virtual, 2020. Available
449 at:
450 [https://www.aeolus.esa.int/confluence/display/CALVAL/Aeolus+NWP+impact+working
451 +meeting+2?preview=/12354328/12354463/5_DWD_acress_aeolus_20200617.pdf](https://www.aeolus.esa.int/confluence/display/CALVAL/Aeolus+NWP+impact+working+meeting+2?preview=/12354328/12354463/5_DWD_acress_aeolus_20200617.pdf).

452 Daley R.: Atmospheric data analysis. Cambridge University Press, Cambridge, 457 pp., ISBN-13
453 978-0521458252, 1991

454 de Kloe, J. and Coauthors: Aeolus Data Innovation Science Cluster DISC ADM-Aeolus Level-
455 2B/2C Processor Input/Output Data Definitions Interface Control Document. *Tech. rep.*,
456 KNMI, Aeolus, DISC, REF: AED-SD-ECMWF-L2B-037, 2020. Available at:
457 [https://earth.esa.int/eogateway/documents/20142/37627/Aeolus-L2B-2C-Input-Output-](https://earth.esa.int/eogateway/documents/20142/37627/Aeolus-L2B-2C-Input-Output-DD-ICD.pdf)
458 [DD-ICD.pdf](https://earth.esa.int/eogateway/documents/20142/37627/Aeolus-L2B-2C-Input-Output-DD-ICD.pdf).

459 Deming, W. E.: Statistical adjustment of data, Wiley, NY (Dover Publications edition, 1985).
460 ISBN 0-486-64685-8, 1943.

461 Frost, C. and Thompson S.: Correcting for regression dilution bias: comparison of methods for a
462 single predictor variable, *Journal of the Royal Statistical Society*, Series A 163: 173–190.
463 <https://doi.org/10.1111/1467-985X.00164>, 2000.

464 Garrett, K., Liu, H., Ide, K., Lukens, K., and Cucurull, L.: Updates to Aeolus Impact Assessment
465 on NOAA global NWP. 2nd ESA Aeolus Cal/Val and Science Workshop, Nov 2-6, 2020.
466 Available at:
467 [https://www.dropbox.com/s/cd0r1gz7t77gq0g/Kevin_Garrett_Oral_Evaluation_of_Aeolu](https://www.dropbox.com/s/cd0r1gz7t77gq0g/Kevin_Garrett_Oral_Evaluation_of_Aeolus.pptx?dl=0)
468 [s.pptx?dl=0](https://www.dropbox.com/s/cd0r1gz7t77gq0g/Kevin_Garrett_Oral_Evaluation_of_Aeolus.pptx?dl=0).

469 Garrett K., H. Liu, K. Ide, R. N. Hoffman, and K. E. Lukens: Optimization and Impact Assessment
470 of Aeolus HLOS Wind Data Assimilation in NOAA’s Global Forecast System, *Q. J. R.*
471 *Meteorol. Soc.*, [submitted revised](#), manuscript QJ-21-0307, 2022.

472 Hoffman, R. N., Kumar, K., Boukabara, S., Yang, F., and Atlas, R.: Progress in Forecast Skill at
473 Three Leading Global Operational NWP Centers during 2015–17 as Seen in Summary
474 Assessment Metrics (SAMs), *Wea. Forecasting*, **33**, 1661-1679,
475 <https://doi.org/10.1175/WAF-D-18-0117.1>, 2018.

476 Hollingsworth, A. and Lonnerberg, P.: The statistical structure of short-range forecast errors as
477 determined from radiosonde data. Part I: The wind field. *Tellus*, 38A, Issue 2, p111-136.
478 <https://doi.org/10.3402/tellusa.v38i2.11707>, 1986

479 Kleist, D. T. and Coauthors: Introduction of the GSI into the NCEP Global Data Assimilation
480 System. *Wea. Forecasting*, **24**, 1691–1705, <https://doi.org/10.1175/2009WAF2222201.1>,
481 2009.

482 Lavers, D. A., Zsoter E., Richardson D. S., And Pappenberger L.: An Assessment of the
483 ECMWF Extreme Forecast Index for WaterVapor Transport during Boreal Winter,
484 *Weather and Forecast*, v32, 1667-1674, doi: 10.1175/WAF-D-17-0073.1, 2017.

485 Liu, H., Garrett, K. Ide, K., Hoffman, R. N., and Lukens, K. E.: Bias correction and Error
486 Specification of Aeolus Winds for NOAA Global Data Assimilation System. 2nd ESA
487 Aeolus CAL/VAL and Science Workshop, Nov 2-6, 2020. Available at:
488 [https://www.dropbox.com/s/f518n7n8ouhgwhy/Hui_LIU_Flash_Evaluation_update.pdf?](https://www.dropbox.com/s/f518n7n8ouhgwhy/Hui_LIU_Flash_Evaluation_update.pdf?dl=0)
489 [dl=0](https://www.dropbox.com/s/f518n7n8ouhgwhy/Hui_LIU_Flash_Evaluation_update.pdf?dl=0).

490 Liu H., K. Garrett, K. Ide, R. N. Hoffman, and K. E. Lukens: Impact Assessment of Aeolus
491 Winds on NOAA Global Forecast, European Geophysical Union general assembly, 19-30
492 Apr 2021. Available at: <https://meetingorganizer.copernicus.org/EGU21/session/40837>.

493 Marseille, G.-J., de Kloe, J., Marksteiner, U., Reitebuch, O., Rennie, M. & de Haan, S.: (2022)
494 NWP calibration applied to Aeolus Mie channel winds. *Quarterly Journal of the Royal*
495 *Meteorological Society*, 1–15. Available from: <https://doi.org/10.1002/qj.4244>, 2022

496 Markovsky I. and Van Huffel S.: Overview of total least squares methods. *Signal Processing*, vol.
497 87, pp. 2283–2302. doi: 10.1016/j.sigpro.2007.04.004, 2007.

498 Reitebuch, O., Bracci, F., and Lux, O.: Assessment of the Aeolus performance and bias correction
499 - results from the Aeolus DISC. 2nd Aeolus Cal/Val Workshop, Nov. 2020. Available at:
500 [https://www.dropbox.com/s/m3kjp540otwm171/Oliver_Reitebuch_Oral_Assessment-](https://www.dropbox.com/s/m3kjp540otwm171/Oliver_Reitebuch_Oral_Assessment-Aeolus-DISC.pdf?dl=0)
501 [Aeolus-DISC.pdf?dl=0](https://www.dropbox.com/s/m3kjp540otwm171/Oliver_Reitebuch_Oral_Assessment-Aeolus-DISC.pdf?dl=0).

502 Rennie, M. P., Isaksen, L., Weiler, F., de Kloe, J., Kanitz, T. and Reitebuch, O.: The impact of
503 Aeolus wind retrievals on ECMWF global weather forecasts, *Q. J. R. Meteorol. Soc.*, pp.
504 ~~1–32~~[147, 3555–3586](https://doi.org/10.1002/qj.4142), doi:10.1002/qj.4142, 2021.

505 Ripley, B. D. and Thompson M.: Regression techniques for the detection of analytical bias,
506 *Analyst*, 112, 377–383. doi: 10.1039/AN987120037, 1987.

507 Straume-Lindner, A. G.: Aeolus Sensor and Product Description'. *Tech. rep.*, European Space
508 Agency - European Space Research and Technology Centre, The Netherlands. REF: AE-
509 SU-ESA-GS-000. Available at:
510 [https://earth.esa.int/eogateway/documents/20142/37627/Aeolus-Sensor-and-Product-](https://earth.esa.int/eogateway/documents/20142/37627/Aeolus-Sensor-and-Product-Description.pdf)
511 [Description.pdf](https://earth.esa.int/eogateway/documents/20142/37627/Aeolus-Sensor-and-Product-Description.pdf), 2018.

512 Straume, A.G. and coauthors: ESA's Space-Based Doppler Wind Lidar Mission Aeolus First
513 Wind and Aerosol Product Assessment Results. Edited by D. Liu, Y. Wang, Y. Wu, B.

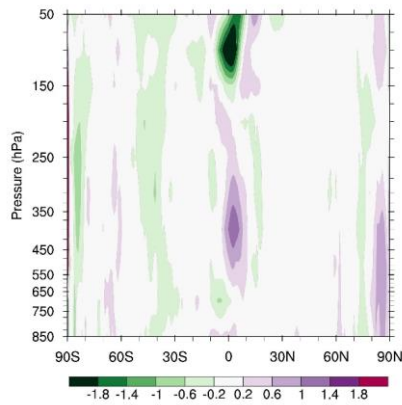
514 Gross, and F. Moshary. EPJ Web of Conferences 237: 01007,
515 <https://doi.org/10.1051/epjconf/202023701007>, 2020.

516 Tan, D. G. H. and others: The ADM-Aeolus wind retrieval algorithms, *Tellus A*, 60, 191-205.
517 [doi:10.1111/j.1600-0870.2007.00285.x](https://doi.org/10.1111/j.1600-0870.2007.00285.x), 2008.

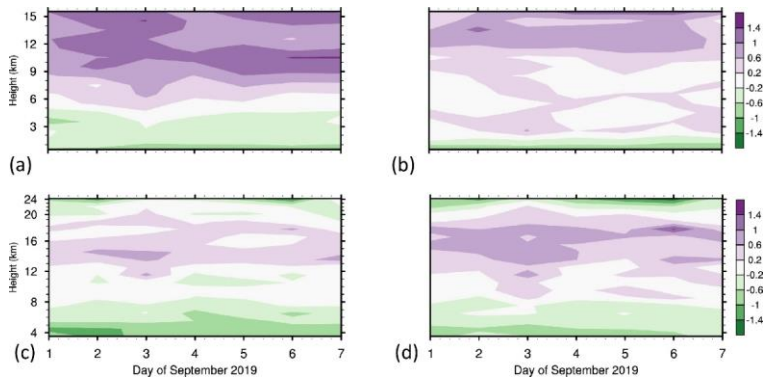
518 Wang, X. and Lei, T.: GSI-Based Four-Dimensional Ensemble–Variational (4DEnsVar) Data
519 Assimilation: Formulation and Single-Resolution Experiments with Real Data for NCEP
520 Global Forecast System. *Mon. Wea. Rev.*, **142**, 3303–3325,
521 <https://doi.org/10.1175/MWR-D-13-00303.1>, 2014.

522 Weiler F. M. Rennie, T. Kanitz, L. Isaksen, E. Checa, Jos de Kloe, O. Reitebuch: Correction of
523 wind bias for the lidar on-board Aeolus using telescope temperatures, *Atmos. Meas. Tech.*
524 [doi: 10.5194/amt-2021-171](https://doi.org/10.5194/amt-2021-171), 2021.

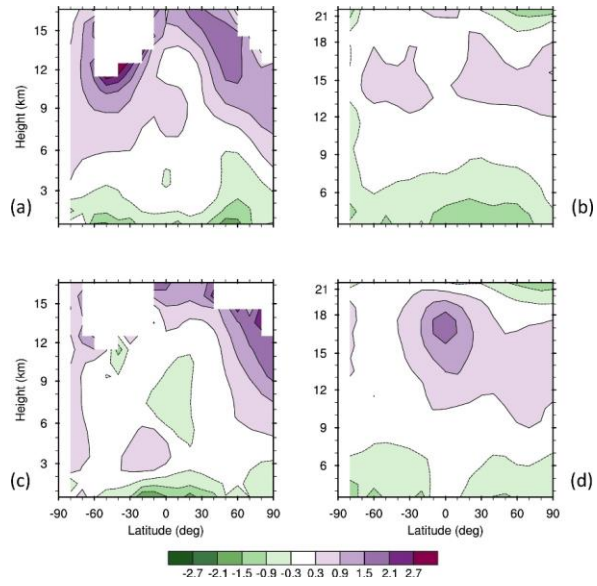
525 **8 Figures**



526
527 Figure 1. Zonal and time mean difference of ECMWF minus FV3GFS backgrounds (defined as 6-h
528 forecasts) for analysis times 00, 06, 12, and 18 UTC for zonal wind (m/s) ~~for~~. Note that in Figs. 1-15 the
529 sample is 1-7 September 2019.



530
531 Figure 2. Vertical and daily variations of global horizontal means of Aeolus winds minus FV3GFS
532 background winds/biases (m/s) for Mie winds (a, b) and Rayleigh winds (c, d) in ascending (a, c) and
533 descending (b, d) orbits.

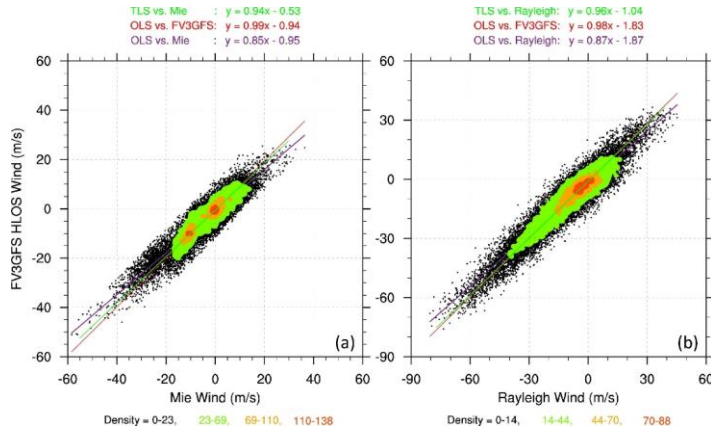


534

535 Figure 3. Latitudinal and height distributions of mean differences (color scale, m/s) of Mie minus
 536 FV3GFS background wind biases (a, c) and Rayleigh minus FV3GFS background wind biases (b, d)
 537 (color scale, m/s) in ascending (a, b) and descending (c, d) orbits for 1-7 September 2019.

538

539

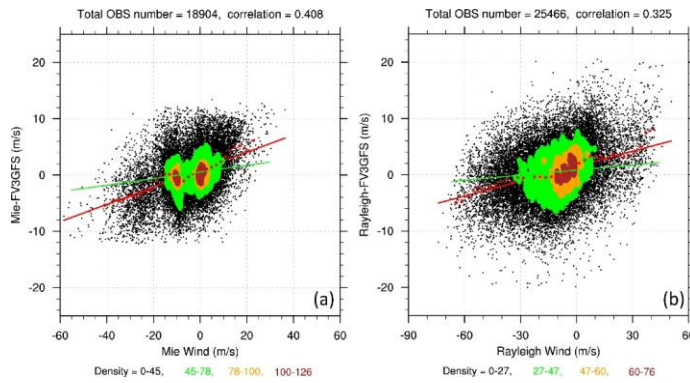


540

541 Figure 4. Density plots of global collocated (a) Mie and FV3GFS winds in the layer at ~3.5 km altitude,
542 and (b) Rayleigh and FV3GFS winds in the layer at ~15 km altitude in descending orbits. The TLS analysis
543 lines (green), the OLS regression lines of FV3GFS winds on Aeolus winds (red), and the OLS regression
544 lines of Aeolus winds on FV3GFS winds (transformed and plotted as a function of Aeolus winds in brown)
545 are shown, with corresponding regression coefficients displayed above each panel.

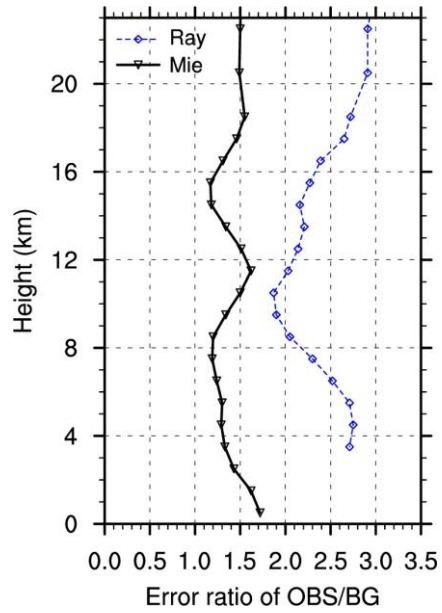
546

547

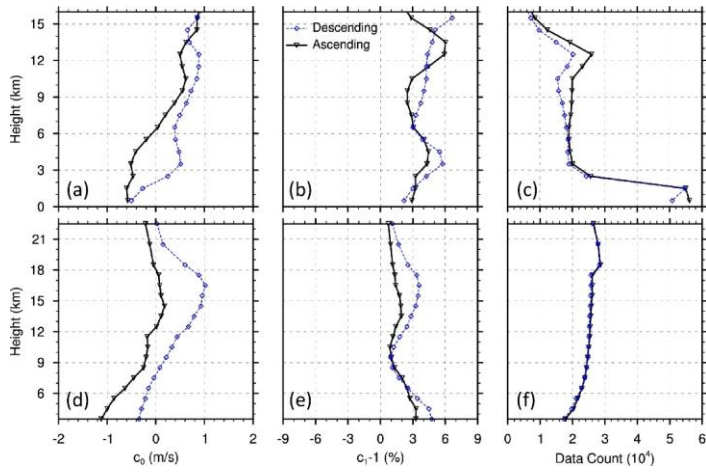


548

549 Figure 5. Density plots of global (a) Mie - FV3GFS winds in the layer at ~3.5 km altitude, and (b) Rayleigh
550 - FV3GFS winds in the layer at ~15 km altitude in descending orbits. The average \ominus -Binnovation (red
551 dots), the OLS regression lines of the innovations on Aeolus winds (red), and TLS analysis lines (green)
552 are shown.



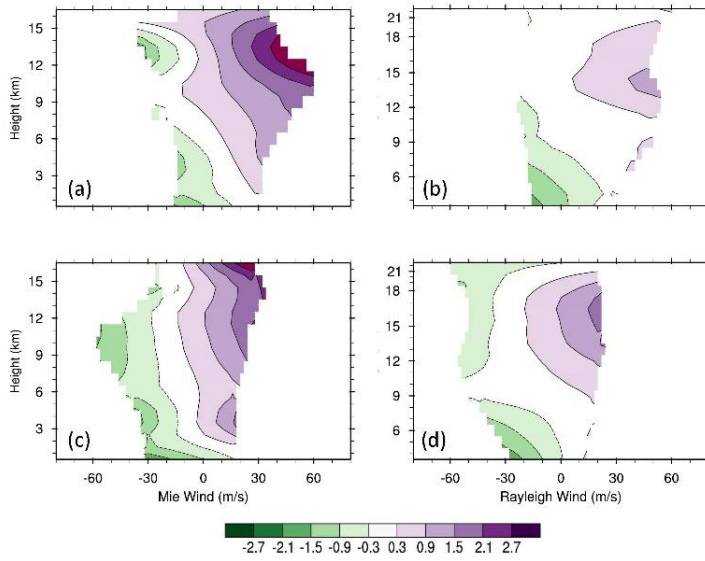
553
 554 Figure 6. Vertical variation of the square root of the ratio of random error variance in [Aeolus winds versus](#)
 555 [FV3GFS background winds](#) for Mie (solid black) and Rayleigh (dashed blue) [Aeolus winds versus FV3GFS](#)
 556 winds. Results are based on global [Aeolus minus FV3GFS winds innovations](#) from the BASE experiment
 557 using Hollingsworth-Lonnberg method. The symbols are plotted at [averaged the average height of the](#)
 558 [observations](#) in each [vertical](#)-layer.



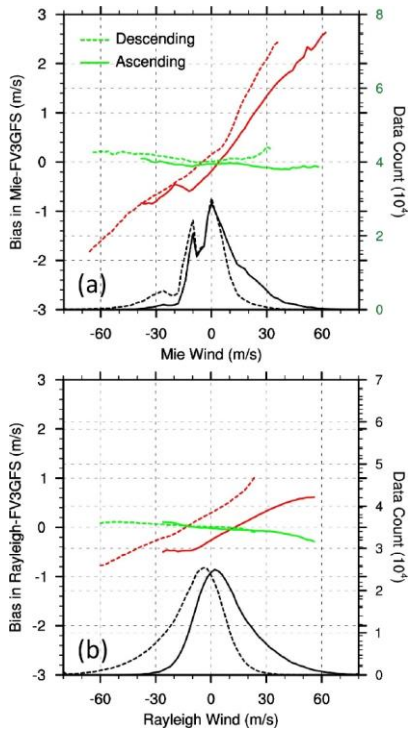
559

560

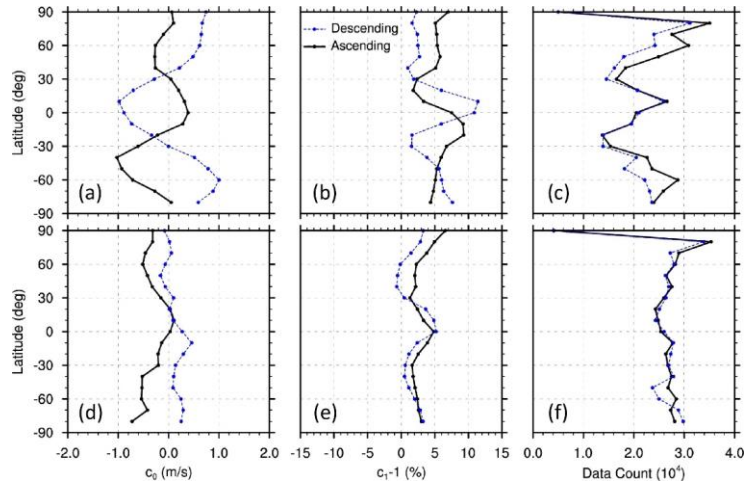
561 Figure 7. Vertical variations of TLS bias coefficients for Mie ~~versus FV3GFS winds~~ (a, b, c), and Rayleigh
 562 ~~versus FV3GFS winds~~ (d, e, f) winds. Each point plotted represents a separate TLS analysis for all
 563 observations in each layer for all latitudes and for either ascending (black solid) or descending (blue dashed)
 564 orbits. The symbols are plotted at the average height of the observations in each layer.



565
 566 Figure 8. Vertical distributions of average TLS estimated biases (color scale, m/s) for ~~innovations of Mie~~
 567 ~~minus FV3GFS winds~~ Mie (a, c) and Rayleigh ~~minus FV3GFS winds~~ (b, d) winds as a function of
 568 observed Aeolus winds (m/s) in ascending (a, b) and descending (c, d) orbits for all latitudes. ~~The TLS~~
 569 ~~estimated biases are~~ obtained from the TLS fits displayed in ~~Figure~~ Fig. 7.



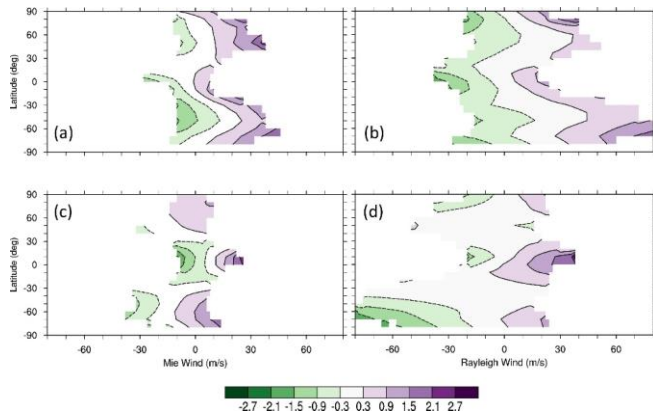
570
 571 Figure 9. TLS estimated biases (m/s) before (red lines) and after (green lines) TLS bias correction for
 572 innovations of Mie minus FV3GFS winds (a) and Rayleigh minus FV3GFS winds (b) as a function
 573 of the observed Aeolus winds (m/s), vertically averaged for all latitudes of Aeolus winds. The black lines
 574 report the number of Aeolus winds in each 2 m/s bin.



575
 576 Figure 10. Latitudinal variation of TLS bias coefficients for innovations of Mie minus FV3GFS winds (a, b, c) and for Rayleigh minus FV3GFS winds (d, e, f) winds. Each point plotted represents a separate
 577 TLS analysis for all observations in all vertical layers in a 10° latitude band for either ascending (black
 578 solid) or descending (blue dashed) orbits. The latitude bands are centered every 10° from 90°S to 90°N.
 579 The symbols are plotted at the center in each latitude band. The vertical layers are 0-16 km for Mie winds
 580 and 3-22 km for Rayleigh winds.

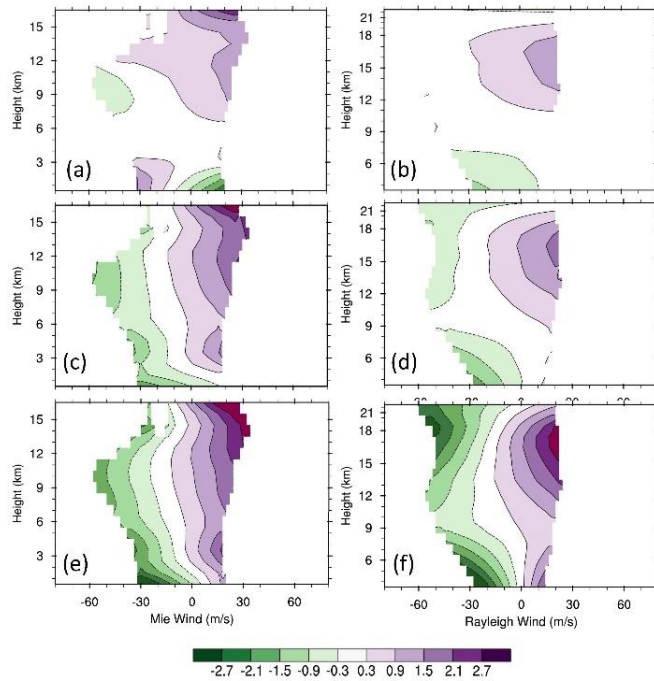
582

583

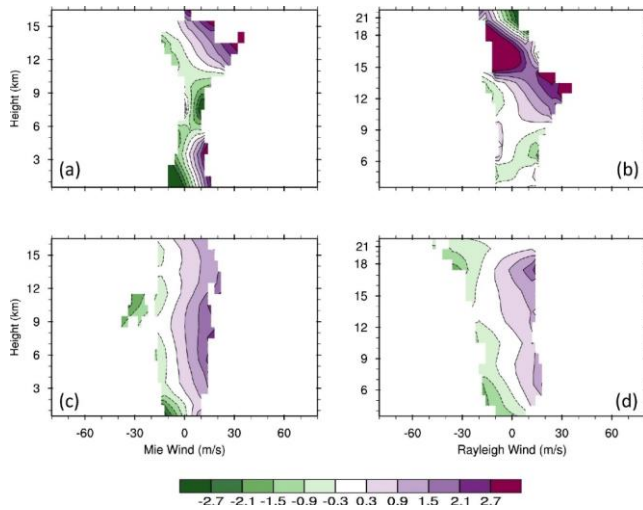


584

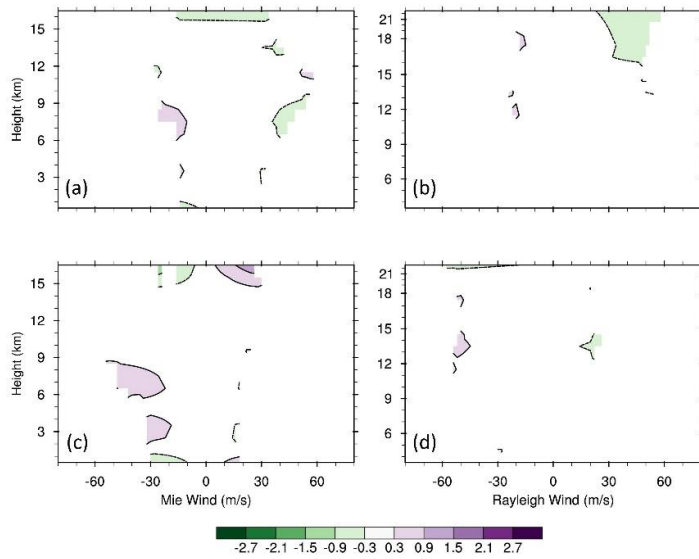
585 Figure 11. Latitudinal distributions of average TLS estimated biases (color scale, m/s) for ~~innovations of~~
586 ~~Mie minus FV3GFS winds~~Mie (a, c) and Rayleigh ~~minus FV3GFS winds~~ (b, d) ~~winds~~ as a function of
587 Aeolus wind in ascending (a, b) and descending (c, d) orbits, obtained from the TLS fits displayed in
588 ~~Figure~~Fig. 10.



589
 590 Figure 12. Vertical distributions of average bias estimates (color scale, m/s) ~~in innovations of~~ Mie ~~minus~~
 591 ~~FV3GFS winds~~ (a, c, e) and Rayleigh ~~minus FV3GFS winds~~ (b, d, f) ~~winds~~ as a function of Aeolus winds
 592 using one of three methods for descending orbits for all latitudes. The methods are OLS using FV3GFS
 593 winds as a predictor (a, b), TLS (c, d, same as the bottom panels of ~~Figure Fig. 8~~), and OLS using the average
 594 of Aeolus and FV3GFS as a predictor (e, f).

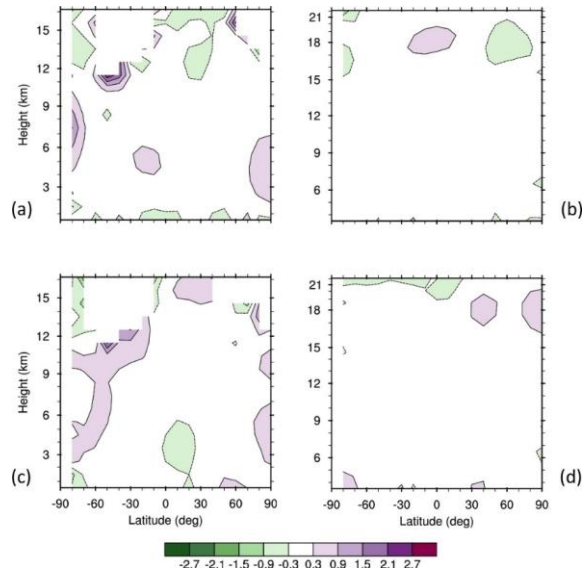


595
 596 Figure 13. Vertical distributions of average TLS estimated biases (color scale, m/s) for Mie minus FV3GFS
 597 winds (a, c) and Rayleigh minus FV3GFS winds (b, d) winds as a function of Aeolus winds (m/s) in the
 598 latitudinal bands centered at Equator (a, b) and at 80S (c, d) for the descending orbits.



599

600 Figure 14. As in [Figure Fig. 8](#) but for the mean innovation after the TLS bias correction is applied. For each
 601 6-h cycle during 1-7 September 2019, the TLS bias correction is calculated from the 28 preceding 6-h
 602 cycles.

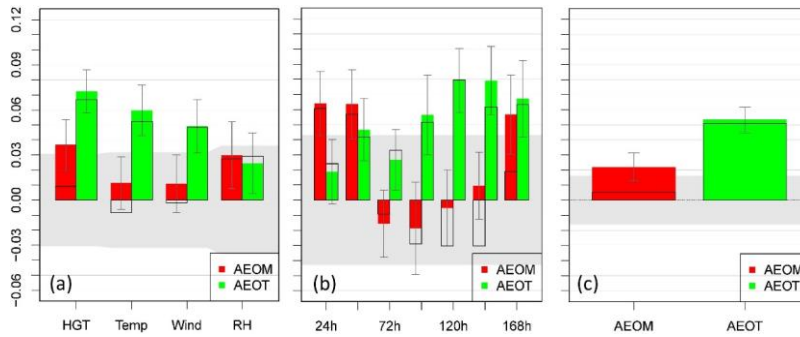


603

604 Figure 15. As in [Figure 3](#) but after the TLS bias correction is applied.

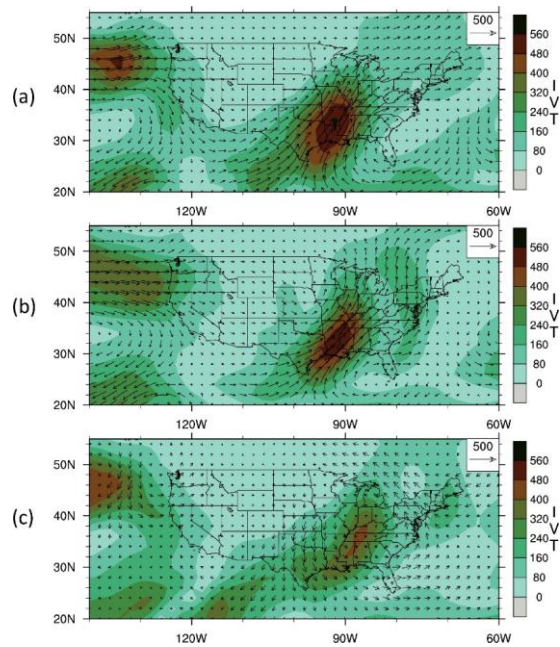
605

606

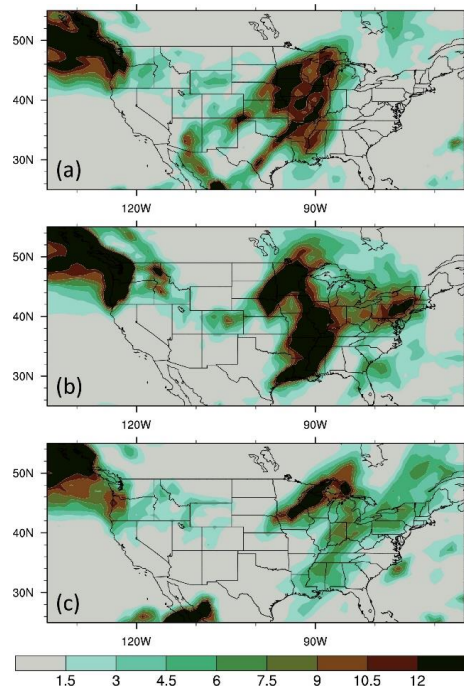


607

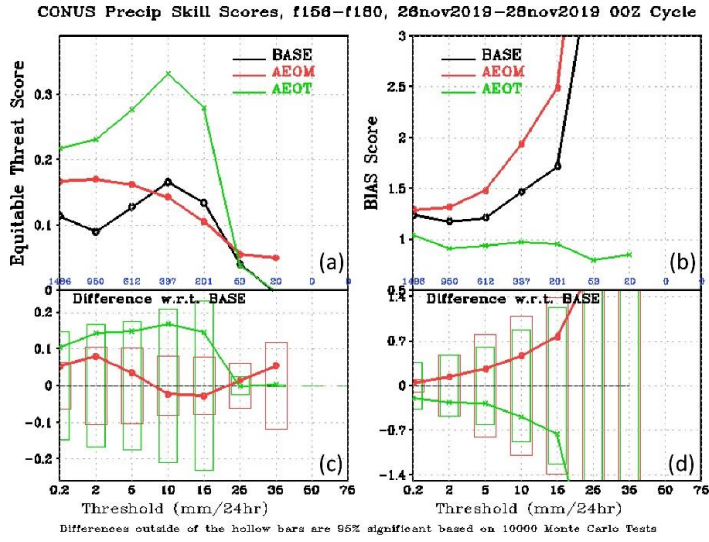
608 Figure 16. The Summary Assessment Metric (SAM) overall forecast scores for AEOM, and AEOT versus
609 BASE experiments. The scores are shown for (a) forecast parameters of temperature (Temp), geopotential
610 height (HGT), vector-wind (Wind) and relative humidity (RH), (b) lead times, and (c) overall
611 performance of AEOM and AEOT. The forecasts are verified to their self-analyses. Values above 0.0
612 demonstrate an increase in the mean of the normalized distribution and improvement of the forecast
613 versus the BASE, while the shaded region represents the 95% significance level. The grey areas indicate
614 the 95% confidence level under the null hypothesis that there is no difference between experiments for
615 this metric. In addition, the estimated uncertainty at the 95% level is indicated by small error bars at the
616 ends of the color bars. Two normalizations are used, the ECDF (colors) and rescaled-minmax
617 normalization (black outline). Details in Hoffman et al. (2018). A value of 0.02, for example, indicates the
618 average normalized statistic over all statistics is better (greater) by 0.02 than BASE. Under the null
619 hypothesis that there are no differences, all SAMs would be 1/2, so a 0.02 improvement can be considered
620 a 4% improvement (0.02/0.5) in normalized scores.



621
 622 Figure 17. The 200-1000 hPa vertically integrated water vapor transport (IVT, kg/m/s, contour) and wind
 623 vectors (m/s, arrows) in the day-7 forecasts, validated at 0000 UTC 26-28 November 2019 and averaged
 624 for (a) BASE, (b) AEOM, (c) AEOT.



625
 626 Figure 18, The 24-h accumulated precipitation (mm) for 156 h to 180 h, averaged for the forecasts
 627 validated from 1200 UTC 26 to 28 ~~+200 UTC~~ November 2019 for (a) BASE, (b) AEOM, (c) AEOT.



628
 629 Figure 19. The forecast skill scores for 24-h accumulated precipitation for Day -7 forecasts validated
 630 from 1200 UTC 26 to 28 1200 UTC-November 2019. The Equitable Threat and BIAS score are measures
 631 of the forecast skill for location and amount of precipitation, respectively. Larger Equitable Threat scores
 632 and BIAS scores closer to 1.0 indicate improved precipitation forecast skill.